COMPENSATION OF MRI T_1-WEIGHTED SPIN-ECHO IMAGES FOR RADIO-FREQUENCY INHOMOGENEITIES

Guylaine Collewet[a,b], Jérôme Idier[b]

[a]Cemagref
17, av de Cucillé, CS 64427, 35044, Rennes, France
phone: + (33)223482167, fax: + (33)223482115, email: guylaine.collewet@cemagref.fr
[b]IRCCyN
1 rue de la Noë, BP 92101, 44321 Nantes Cedex 3, France
phone: + (33)240376909, fax: + (33)240376930, email: Jerome.Idier@irccyn.ec-nantes.fr
web: http://www.irccyn.ec-nantes.fr/~idier

ABSTRACT

We propose a correction method for magnetic resonance (MR) images to eliminate the effects of the inhomogeneity of the radio-frequency (RF) pulses and of the sensivity of the RF reception particularly in the case of T_1-weighted images. In this case the effects of the pulse inhomogeneities vary with the tissues, which prevents the use of simpler correction techniques based on a global multiplicative bias field model. Here, the MR signal is modeled as a sum of contributions of all the tissues present in the object. For sake of generality, each pixel is assumed to contain an unknown proportion of each tissue, so that the usually adopted segmentation based approach is not valid in the present context. The number of tissues composing the object as well as the MR characteristics of each tissue are required. Several images with different acquisition parameter values are also needed. A penalized least-square criterion is proposed to estimate the RF emitted field, the RF sensitivity reception and the proportion of each tissue. The criterion contains smoothness regularization for both RF fields. We solve the optimization problem using a conjugate gradient algorithm within a Gauss-Seidel iterative scheme. Results based on real MR images of fish demonstrate the effectiveness of the method.

1. INTRODUCTION

Magnetic resonance imaging (MRI) is an advanced technique providing valuable information in various kinds of applications such as medical diagnosis, food products analysis [1] or the study of fluids in porous materials [2]. MRI can be used for visual inspection, but it is sometimes needed to get some quantitative information from the images. However, the process of MR image formation introduces various artefacts which may corrupt the information expected to be retrieved from the images. A correction algorithm is then needed to overcome this problem.

The artefacts in MRI can be divided in two categories, whether they corrupt the localisation of the signal or not.

The MR signal is the sum of the RF signals issued from all the protons positionned in the permanent magnetic field B_0, and experimenting a sequence of pulses of RF magnetic field. This signal is acquired through a coil. A gradient of magnetic field $G(r)$ that linearly depends on the position r is added to B_0. As the signal frequency of the protons is proportional to $B_0 + G(r)$, the protons can be located thanks to the Fourier transform which computes the amplitude of each frequency [3]. However, inhomogeneities of permanent field and of the gradients generate signal localisation artefacts. These artefacts can be neglected in the case of low-field MR imaging, which is the frame of our work, with the use of sequences of RF pulses such as spin-echo.

On the other hand, two phenomena produce artefacts that do not affect the localisation but introduce spatial variations in the signal intensity:

- The sensitivity of the RF reception (RFR) coil is not homogeneous.
- Spatial inhomogeneities of the RF emission coil, coupled with off-resonance phenomenon linked to B_0 inhomogeneities, produce spatial variations of applied RF pulses (RFP), which in turn influence the signal intensity [4].

The inhomogenities due to RFP and RFR influence the image formation process in two different ways. The RFR effect can be considered as a multiplicative bias, while the influence of RFP depends on the proton longitudinal relaxation times T_1, particularly in spin-echo T_1-weighted images [5]. Such images are commonly used in MR applications, since the contrast between tissues with different T_1 can be enhanced using appropriate values of the repetition time TR. For example, this is the case for brain tissues (*i.e.,* gray matter, white matter and cerebrospinal fluid) or for fat and muscle.

Different approaches to the global problem of RF inhomogeneities can be found in the literature [6]. Some of them try to remove low-frequency variations of the signal. This is done with homomorphic filtering in [7, 8], and with a more sophisticated method where the bias field and the intensity distribution of the tissues are iteratively estimated in [9]. However, such approaches are not suited to applications where the low-frequency variations of the signal are partly due to the object itself. In order to incorporate a priori information, many authors proposed methods for the estimation of the bias field based on tissue segmentation. The expectation-maximization algorithm (EM) is used in [10] to alternately estimate the bias and the statistical characteristics of each tissue. This algorithm was improved in [11] thanks to the modeling of partial volume. EM was also chosen in [12], where additional morphological information was taken from an atlas. Finally, some authors consider a Markov random field model to describe spatial correlations [13, 14]. These methods make the assumption that each pixel contains only one kind of tissue. While this is well-suited to the important case of cerebral imaging, it does not correspond to the general situation, as found for example in MRI muscle ex-

amination [15], or in food products analysis such as fish [16] or bread [17].

Finally, some authors proposed to use additional images in their correction scheme. In [18–21], images of phantoms were used as exact images of the bias field. An interesting hybrid approach is proposed in [22] in the particular case of surface coils. An additional body coil image is then used, which is supposed homogeneous but with low signal intensity. Compared to the previously mentioned methods, the latter ones rely on weaker assumptions on the object. However, they all share the same simplistic model of bias, considered as a smoothly varying, multiplicative component. As a consequence, they neglect the dependence between the T_1 of the tissues and the RFP inhomogeneities.

In this paper, we introduce a method that makes no additional assumption on the morphology of the imaged object, while the particular effect of the RFP inhomogeneities linked to the T_1 is taken into account. As a price to pay for generality, several images of the same object are needed[1], for different acquisition parameter values. Moreover the tissues composing the object are supposed to be known.

The paper is organized as follows: In Section 2 we derive the mathematical model behind our method. In Section 3 the solution of the optimisation problem is detailed. Section 4 is dedicated to results obtained on real images acquired on a low-field imager. They demonstrate the efficiency of the method in the case of fish. Finally some perspectives are proposed in Section 5.

2. PROBLEM FORMULATION

2.1 Signal model

2.1.1 Case of a one-tissue homogeneous object

In the simplified case of an homogeneous object containing only one tissue and under hypotheses detailed in [23], the noise-free spin-echo intensity s_ℓ at pixel $\ell = 1,\dots,N$ can be modeled by:

$$s_\ell = R_\ell O f(\eta_\ell, \alpha, \beta, TR, T_1)$$

with

$$f(\eta_\ell, \alpha, \beta, TR, T_1) = \frac{1}{2}\frac{\sin \eta_\ell\alpha(1-\cos\eta_\ell\beta)(1-E_1)}{1-E_1\cos\eta_\ell\alpha\cos\eta_\ell\beta}, \quad (1)$$

where $E_1 = \exp(-TR/T_1)$. $\boldsymbol{R} = (R_\ell)$ represents the reception coil sensitivity, $\eta = (\eta_\ell)$ the attenuation factor for the nominal pulse angle, α the flip angle, β the angle of the refocusing pulse, O the signal that corresponds to $(\boldsymbol{R}, \eta, \alpha, \beta) = (\mathbf{1}, \mathbf{1}, 90°, 180°)$, and T_1 the longitudinal relaxation time of the tissue.

This model shows the multiplicative effect of RFR inhomogeneities represented by $\boldsymbol{R}$ and also the link between T_1 and the RFP inhomogeneities represented by η. The function f takes different values in function of T_1 for non-zeros values of E_1. This is the case in T_1-weighted images, where TR is short compared to T_1.

In order to cope with realistic situations, this model must be extended to the case of objects that are made of several components (or tissues).

[1] Additional images of phantoms composed of the relevant tissues are also suited.

2.1.2 General case of an object composed of several tissues

Let us consider an object composed of N_t tissues (*e.g.,* fat, muscle, grey and white matter, ...), in the case of spin-echo sequence where the additivity of the signals is valid. Then, for each pixel, the noise-free signal can be modeled by:

$$s_\ell = R_\ell \sum_{i=1}^{N_t} k_{i\ell} O_i f(\eta_\ell, \alpha, \beta, TR, T_{1i})$$

where $k_{i\ell} \in [0,1]$ is the proportion of tissue i in pixel ℓ, O_i the signal for $k_{i\ell} = 1$ and $(R_\ell, \eta_\ell, \alpha, \beta) = (1, 1, 90°, 180°)$, and T_{1i} the longitudinal relaxation time of tissue i. Moreover, if we consider that pixels are filled with tissues, *i.e.,* if we exclude the case of pixels partially containing air, the following relation is verified :

$$\sum_{i=1}^{N_t} k_{i\ell} = 1, \qquad \forall \ell = 1,\dots,N. \quad (2)$$

Our goal is to retrieve the signal s^* that would be issued from a perfect MR system, that is for $(\boldsymbol{R}, \eta) = (\mathbf{1}, \mathbf{1})$:

$$s^*_\ell = \sum_{i=1}^{N_t} k_{i\ell} O_i f(1, \alpha, \beta, TR, T_{1i}).$$

(α, β, TR) can be considered as known constants chosen by the MR operator.

Since $\boldsymbol{R}$ and $\boldsymbol{O} = (O_i)$ are linked multiplicatively, all couples $(C\boldsymbol{R}, \boldsymbol{O}/C)$ (with $C > 0$) are equivalent from the measurement viewpoint. To raise this undeterminacy, we propose to assume that the quantities O_i are known, since they can be measured during a calibration step. For example, the intensity of regions containing only one tissue can be measured manually once for all. We also rely on a sufficiently good knowledge of T_{1i}, since relaxation times can be precisely measured using NMR experiments. Thus the remaining unknown variables are $\boldsymbol{R} = (R_\ell)$, $\eta = (\eta_\ell)$ and $\boldsymbol{k} = (k_{i\ell})$, which amounts to $N_t + 2$ images, *i.e.,* $(N_t + 1) \times N$ scalar unknowns given constraint (2). In order to build reliable estimates, we propose to acquire $N_s \geqslant N_t + 1$ images $\boldsymbol{s}_j = (s_{j\ell})$, using different values for the triple $\theta = (\alpha, \beta, TR)$. Such a procedure necessarily increases the acquisition time compared to the acquisition of a single image. In this respect, it is interesting to use short TR, as the acquisition time of one image is directly proportional to this parameter.

2.2 Cost function definition

Noise in MR magnitude images is governed by a Rician distribution [24]. However for signal to noise ratio greater than 3, which is the case in most applications, it can be considered as white Gaussian. Thus we propose to estimate $\boldsymbol{R}$, $\boldsymbol{k}$ and η by joint minimization of a penalized least-square cost function:

$$(\hat{\boldsymbol{R}}, \hat{\boldsymbol{k}}, \hat{\eta}) = \arg\min_{\boldsymbol{R},\boldsymbol{k},\eta} J(\boldsymbol{R}, \boldsymbol{k}, \eta) \quad \text{s.t.} \quad \sum_{i=1}^{N_t} k_{i\ell} = 1, \quad (3)$$

where

$$J(\boldsymbol{R}, \boldsymbol{k}, \eta) = \sum_{j=1}^{N_s} \lambda_j \sum_{\ell=1}^{N} \left(\mathbf{s}_{j\ell} - R_\ell \sum_{i=1}^{N_t} O_i k_{i\ell} f(\eta_\ell, \theta_j, T_{1i}) \right)^2 + \delta \|\mathbf{D}\boldsymbol{R}\|^2 + \gamma \|\mathbf{D}\eta\|^2. \quad (4)$$

Parameters λ_j, δ and γ are positive weights and $\mathbf{D}$ represents a finite difference operator. The first term in (4) accounts for data fidelity. The second and third terms ensure that $\hat{\boldsymbol{R}}$ and $\hat{\eta}$ are reasonably smooth, given the antennae configuration [25].

3. SOLUTION OF THE OPTIMIZATION PROBLEM

Let $\boldsymbol{R}' = (R'_\ell)$ with $R'_{i\ell} = R_i k_{i\ell}$, so that $\boldsymbol{R}$ and $\boldsymbol{k}$ can be retrieved from $\boldsymbol{R}'$ given (2) according to:

$$R_\ell = \sum_{i=1}^{N_t} R'_{i\ell}, \qquad k_{i\ell} = \frac{R'_{i\ell}}{R_\ell}.$$

It is easy to check that the minimization problem (3)-(4) takes the following simpler form in terms of $(\boldsymbol{R}', \eta)$: $(\hat{\boldsymbol{R}}', \hat{\eta}) = \arg\min_{\boldsymbol{R}', \eta} J'(\boldsymbol{R}', \eta)$, where

$$J'(\boldsymbol{R}', \eta) = \sum_{j=1}^{N_s} \lambda_j \sum_{\ell=1}^{N} \left(\mathrm{s}_{j\ell} - \sum_{i=1}^{N_t} O_i R'_{i\ell} f(\eta_\ell, \theta_j, T_{1i}) \right)^2 + \delta \left\| \mathbf{D} \sum_{i=1}^{N_t} \boldsymbol{R}'_i \right\|^2 + \gamma \|\mathbf{D}\eta\|^2, \quad (5)$$

with $\boldsymbol{R}'_i = (R'_{i\ell}, \ell = 1, \ldots, N)$. In particular, the new formulation is no more constrained. Moreover, (5) is a quadratic function of $\boldsymbol{R}'$.

We propose to resort to a coordinate descent approach to compute $\hat{\boldsymbol{R}}'$ and $\hat{\eta}$:

1. While η is held at its current value, a fixed number of iterations of a conjugate gradient algorithm are performed to minimize J' as a function of $\boldsymbol{R}'$.
2. While $\boldsymbol{R}'$ is held at its current value, a fixed number of iterations of a conjugate gradient algorithm are performed to minimize J' as a function of η.

Steps 1 and 2 are performed repeatedly, until the norm of the gradient of J' with respect to $(\boldsymbol{R}', \eta)$ becomes sufficiently small, *i.e.,* $\|\nabla J'(\boldsymbol{R}', \eta)\| \leqslant \varepsilon$. Although the two steps look very similar, the second one is practically more complex since (1) is a nonlinear, multimodal function of η. As a consequence, J' may possess local minima. In practice, it is hoped that proper initialisation of η allows to converge towards the global minimum. The expected values vary approximatively between 0.6 and 1.3, and it is reasonable to take $\eta = \mathbf{1}$ as initial point. Remark that the initial value of $\boldsymbol{R}'$ can remain arbitrary, provided that the first instance of Step 1 is performed until practical convergence.

According to the probabilistic interpretation of criterion J', λ_j corresponds to the inverse of the noise variance for the jth image. The noise variances can be estimated directly from the images using the method proposed in [26]. The remaining parameters δ and γ are chosen empirically at the present stage of our work.

4. RESULTS

4.1 Image acquisition

We used a trout to test our algorithm, with a view to an application to food science. Fish is a convenient model as it is made of two tissues, fat and muscle, with approximatively known T_1. We used $N_s = N_t + 1 = 3$ different images.

- $\boldsymbol{s}_1$ was acquired on the trout with $(\alpha, \beta, TR) = (90°, 180°, 140$ ms). Such parameter values produce T_1weighted images since the TR value is short enough regarding the T_1 values of fat and muscle. These values were evaluated by NMR measurements as 100 ms and 500 ms, respectively. Five different images $\boldsymbol{s}_1^1, \ldots, \boldsymbol{s}_1^5$ of the same slice of the fish were actually acquired after a translation of 22.5 mm between each acquisition, along the z axis (*i.e.,* perpendicularly to the slice plane).
- $\boldsymbol{s}_2$ (respectively, $\boldsymbol{s}_3$) was acquired on a cylinder filled with oil, with $(\alpha, \beta, TR) = (60°, 180°, 700$ ms) (resp., $(\alpha, \beta, TR) = (120°, 180°, 700$ ms)).

The MRI system was a 0.2 T imager (Open, Siemens). The fish was kept refrigerated at 5°C to avoid signal variations due to temperature. The field of view was 200 mm × 200 mm and the matrix size was $N = 256 \times 256$. The slice thickness was 4 mm for $\boldsymbol{s}_1$ and 10 mm for $\boldsymbol{s}_2$ and $\boldsymbol{s}_3$. The quantities O_i were measured on $\boldsymbol{s}_1$: a region filled with fat was manually defined where the mean intensity was computed. For the muscle signal, a region physiologically known as very low-fat (less than 1%) was chosen as reference.

4.2 Parameter algorithm

No prior information was assumed on the values of $\boldsymbol{R}$, η and $\boldsymbol{k}$. We stopped the coordinate descent when $\|\nabla J'(\boldsymbol{R}', \eta)\|$ became lower than $\varepsilon = 3N \times 10^{-4}$. We run each conjugate gradient with a fixed number of iterations equal to 5. In order to increase the convergence speed, we used an overrelaxation factor of 1.8 for Step 1. The values of λ_j were chosen equal to one, since the three images were about equally noisy. The values of δ and γ were chosen empirically as 10^7.

4.3 Image results

The top row of Figure 1 shows the five images $\boldsymbol{s}_1^1, \ldots, \boldsymbol{s}_1^5$ of the same slice of the trout, acquired at different positions in the MR system. The bottom row displays the corresponding corrected images. The highest gray levels correspond to fat

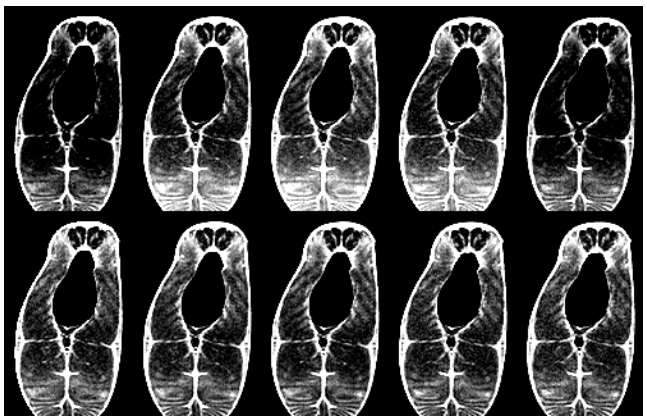

Figure 1: Top row: Original images acquired from left to right at −45 mm, −22.5 mm, 0 mm, 22.5 mm and 45 mm from the centre of the MR system, respectively. Bottom row: corrected images

tissues and the lowest to muscle. Due to the trout physiology and to the relative thickness of the slices, many pixels contain both fat and muscle. Let us remark here that such a

configuration is definitively not suited to segmentation based approaches.

We can clearly see the effects of the RF inhomogeneities on the original images. The two extreme images exhibit lower signals, while all corrected images exhibit a similar range of grey levels. Histograms of signal intensity are presented in Figure 2 for the raw images and in Figure 3 for the corrected images. The histograms of the raw images significantly differ one from each other due to the inhomogeneities, while they are very much alike for the corrected images. As expected, each image exhibits a narrower histogram once corrected.

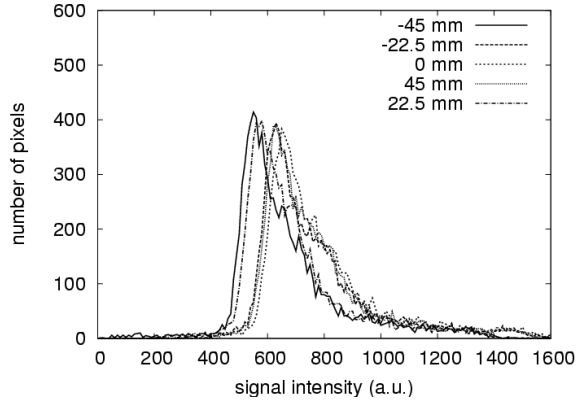

Figure 2: Histograms of signal intensity for the five original images

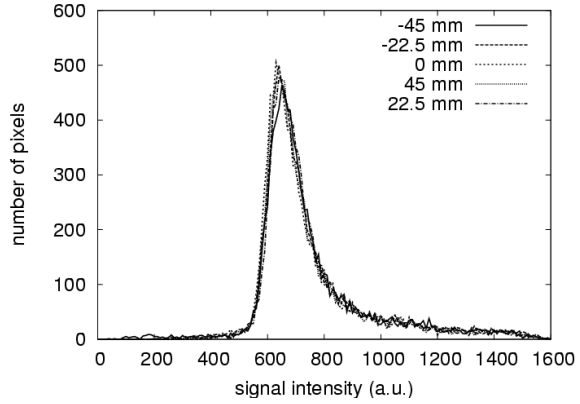

Figure 3: Histograms of signal intensity for the five corrected images

Figure 4 shows the same five images after only partial correction: only $\boldsymbol{R}'$ was estimated and compensated for, while η and f were assumed equal to one. This configuration is equivalent to the modeling of the inhomogeneities by a multiplicative bias field. The result shows that it is not sufficient to estimate the multiplicative bias $\boldsymbol{R}$ only, especially in the zones that contain more muscle. This is particulalry true for the images at -45 mm and -22.5 mm, where low values of η were found. Indeed, the effect of the inhomogeneities of η has a greater influence on the tissue with large T_1 compared to TR. It is the case of fish muscle, with $T_1 = 500$ ms to be compared with $TR = 140$ ms. Figure 5 shows the corresponding histograms, which confirms the visual inspection of Figure 4.

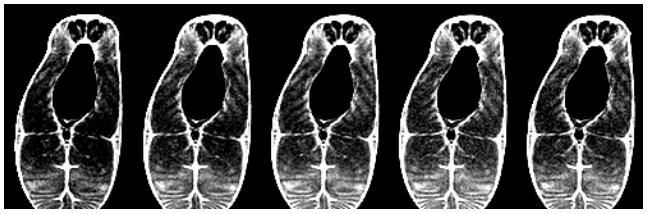

Figure 4: Images corrected without the estimation of η

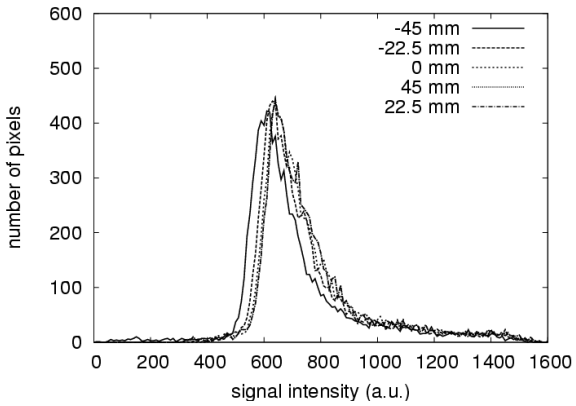

Figure 5: Histograms of signal intensity for the five images corrected without the estimation of η

5. CONCLUSION

We have proposed a correction method for inhomogeneities of RF pulses and RF reception in MR systems. This method is based on the modeling of the signal as a sum of contributions of different tissues, in order to account for the fact that different tissues yield different responses regarding the RF pulse values, particularly in the case of T_1-weighted images.

Our method makes no assumption of piecewise constant regions in the image, which we find too restrictive an assumption. It is rather based on the processing of several images, acquired at different measurement parameter values. The resulting estimation problem pertains to partially nonlinear source separation.

A penalized least-squares criterion was defined to balance a data fidelity term and regularization terms for the RF pulses and reception maps. The resulting method proved to be efficient on a fish slice with a two-tissue model, using a set of three images, two of which being acquired on an oil phantom.

In order to improve the method and to enlarge the potential applications, several points remain to be explored. First, the acquisition time is a key point in MRI. Our method needs at least $N_t + 1$ images in the case of an object made of N_t tissues. The use of images acquired on phantoms once for all does not penalize the acquisition time. However, such images do not account for inhomogeneities due to patient-specific geometrical and electrical properties. Although such a mismatch is of minor effect in low-field imaging, it would be preferable to limit the resort to phantoms, for the sake of

generality. If more images are to be acquired on the object, shorter acquisition times should be used. This could be done with shorter TR or with fast spin-echo sequences to get additional, less accurate images. As our approach is regularized, one can hope that a certain level of degradation in the data will be of limited consequence on the quality of the results.

REFERENCES

[1] B. Hills, *Magnetic resonance imaging in food science*, A Wiley Interscience publication, New York, 1998.

[2] B. Blümich, *NMR imaging of materials*, Monographs on the physics and chemistry of materials. Oxford Univesity Press, 2000.

[3] E. Haacke, R. Brown, M. Thompson, and R. Venkatesan, *Magnetic Resonance Imaging: Physical Principles and Sequence Design*, Wiley-Liss, 1999.

[4] J. G. Sled and G. B. Pike, "Correction for B_1 and B_0 variations in quantitative T_2 measurements using MRI", *MRM*, vol. 43, no. 4, pp. 589–593, 2000.

[5] J. Wang, M. Qiu, and R. Constable, "In vivo method for correcting transmit/receive nonuniformities with phased array coils", *MRM*, vol. 53, no. 3, pp. 666–674, 2005.

[6] B. Belaroussi, J. Milles, S. Carme, Y. M. Zhu, and H. Benoit-Cattin, "Intensity non-uniformity correction in MRI: Existing methods and their validation", *Med. Image. Anal.*, vol. 10, no. 2, pp. 234–246, 2006.

[7] A. Koivula, J. Alakuijala, and O. Tervonen, "Image feature based automatic correction of low-frequency spatial intensity variations in MR images", *MRI*, vol. 15, no. 10, pp. 1167–1175, 1997.

[8] B. H. Brinkmann, A. Manduca, and R. A. Robb, "Optimized homomorphic unsharp masking for MR grayscale inhomogeneity correction", *IEEE Trans. Medical Imaging*, vol. 17, no. 2, pp. 161–171, 1998.

[9] J. G. Sled, A. P. Zijdenbos, and A. C. Evans, "A nonparametric method for automatic correction of intensity nonuniformity in MRI data", *IEEE Trans. Medical Imaging*, vol. 17, no. 1, pp. 87–97, 1998.

[10] W. Wells, R. Kikinis, W. Grimson, and F. Jolesz, "Adaptive segmentation of MRI data", *IEEE Trans. Medical Imaging*, vol. 15, no. 4, pp. 429–422, 1996.

[11] R. Guillemaud and M. Brady, "Estimating the bias field of MR images", *IEEE Trans. Medical Imaging*, vol. 16, no. 3, pp. 238–251, 1997.

[12] S. Prima, N. Ayache, T. Barrick, and N. Roberts, "Maximum likelihood estimation of the bias field in MR brain images : Investigating different modelings of the imaging process", in *MICCAI*. 2001, pp. 818–819, Springer-Verlag Berlin Heidelberg.

[13] Y. Zhang, M. Brady, and S. Smith, "Segmentation of brain MR images through a hidden Markov random field model and the expectation-maximization algorithm", *IEEE Trans. Medical Imaging*, vol. 20, no. 1, 2001.

[14] K. Van Leemput, F. Maes, D. Vandermeulen, and P. Suetens, "Automated model-based bias field correction of MR images of the brain", *IEEE Trans. Medical Imaging*, vol. 18, no. 10, pp. 885–896, 1999.

[15] F. A. Marden, A. M. Connolly, M. J. Siegel, and D. A. Rubin, "Compositional analysis of muscle in boys with duchenne muscular dystrophy using MR imaging", *Skeletal Radiology*, vol. 34, no. 3, pp. 140–148, 2005.

[16] C. Toussaint, B. Fauconneau, F. Medale, G. Collewet, S. Akoka, P. Haffray, and A. Davenel, "Description of the heterogeneity of lipid distribution in the flesh of brown trout (salmo trutta) by MR imaging", *Aquaculture*, vol. 243, no. 1-4, pp. 255–267, 2005.

[17] A. Grenier, T. Lucas, G. Collewet, and A. Le Bail, "Assessment by MRI of local porosity in dough during proving. Theoretical considerations and experimental validation using a spin-echo sequence", *MRI*, vol. 21, no. 9, pp. 1071–1086, 2003.

[18] B. Condon, J. Patterson, D. Wyper, A. Jenkins, and D. Hadley, "Image non-uniformity in magnetic resonance imaging : its magnitude and methods for its correction", *Brit. J. Radiol.*, vol. 60, no. 709, pp. 83–87, 1987.

[19] P. S. Tofts, G. J. Barker, A. Simmons, D. G. Macmanus, J. Thorpe, A. Gass, and D. H. Miller, "Correction of nonuniformity in images of the spine and optic- nerve from fixed receive-only surface coils at 1.5-T", *J. Comput. Assist. Tomogr.*, vol. 18, no. 6, pp. 997–1003, 1994.

[20] E. McVeigh, M. Bronskill, and R. Henkelman, "Phase and sensitivity of receiver coils in magnetic resonance imaging", *Med. Phys.*, vol. 13, no. 6, pp. 806–814, 1986.

[21] M. Tincher, C. R. Meyer, R. Gupta, and D. M. Williams, "Polynomial modeling and reduction of RF body coil spatial inhomogeneity in MRI", *IEEE Trans. Medical Imaging*, vol. 12, no. 2, pp. 361–365, 1993.

[22] A. Fan, M. W. I. William, J. W. Fisher III, c. Müjdat, S. Steven Haker, R. V. Mulkern, C. Tempany, and A. S. Willsky, "A unified variational approach to denoising and bias correction in MR", in *IPMI*, 2003, pp. 148–159.

[23] G. Collewet, A. Davenel, C. Toussaint, and S. Akoka, "Correction of intensity nonuniformity in spin-echo T_1-weighted images", *MRI*, vol. 20, no. 4, pp. 365–373, 2002.

[24] J. Sijbers, A. Den Dekker, J. Van Audekerke, M. Verhoye, and D. Van Dick, "Estimation of the noise in magnitude MR images", *MRI*, vol. 16, no. 1, pp. 87–90, 1998.

[25] J. G. Sled and G. B. Pike, "Understanding intensity non-uniformity in MRI", in *MICCAI*, vol. 1496 of *Lecture Notes in Computer Science*, pp. 614–622. 1998.

[26] R. D. Nowak, "Wavelet-based rician noise removal for magnetic resonance imaging", *IEEE Trans. Medical Imaging*, vol. 8, no. 10, pp. 1408–1419, 1999.